
This is an electronic reprint of the original article.
This reprint may differ from the original in pagination and typographic detail.

Chu, Guang; Chen, Feng; Zhao, Bin; Zhang, Xue; Zussman, Eyal; Rojas, Orlando J.

Self-Assembled Nanorods and Microspheres for Functional Photonics : Retroreflector Meets Microlens Array

Published in:
ADVANCED OPTICAL MATERIALS

DOI:
[10.1002/adom.202002258](https://doi.org/10.1002/adom.202002258)

Published: 05/05/2021

Document Version
Publisher's PDF, also known as Version of record

Published under the following license:
CC BY-NC

Please cite the original version:
Chu, G., Chen, F., Zhao, B., Zhang, X., Zussman, E., & Rojas, O. J. (2021). Self-Assembled Nanorods and Microspheres for Functional Photonics : Retroreflector Meets Microlens Array. *ADVANCED OPTICAL MATERIALS*, 9(9), Article 2002258. <https://doi.org/10.1002/adom.202002258>

This material is protected by copyright and other intellectual property rights, and duplication or sale of all or part of any of the repository collections is not permitted, except that material may be duplicated by you for your research use or educational purposes in electronic or print form. You must obtain permission for any other use. Electronic or print copies may not be offered, whether for sale or otherwise to anyone who is not an authorised user.

Self-Assembled Nanorods and Microspheres for Functional Photonics: Retroreflector Meets Microlens Array

Guang Chu,* Feng Chen, Bin Zhao, Xue Zhang, Eyal Zussman, and Orlando J. Rojas*

Patterned micro/nanomaterials display efficient light management capabilities owing to their control of light propagation within multiscale periodic structures. Here a hierarchical photonic structure composed of polystyrene microspheres and cholesteric assembly of cellulose nanocrystals is described, acting as a polarization-sensitive retroreflective coating and microlens array. Micropatterned photonic films are prepared by casting an aqueous cellulose nanocrystal suspension onto a monolayer of polystyrene microspheres substrate through evaporation-assisted transfer imprinting lithography, integrating a bulk cholesteric matrix and patterned surface. By directing light at the as-assembled polystyrene surface, an enhanced structural color develops from the circularly polarized light retroreflection. Whereas when light travelling across the photonic film, the transparent layer of polystyrene microspheres forms into plano-convex microlens to converge the transmitted light into the focus plane and reduce centimeter-scale illuminated image into a high-fidelity miniaturized replica. This simple method, combining self-assembly with imprinting lithography, is expected to pave the way for designing custom-tailored optics with novel functions.

saturation of such color, while many animals have evolved to detect and make use of light polarization, realizing multiple biological functions in one integrated structure.^[1,2] Some arthropods display polarization-sensitive iridescent structural colors to distinguish themselves from the environment and perform as signal medium for vision, image capture, communication, and mate recognition.^[3–5] The respective photonic structure can selectively reflect circularly polarized light with the same handedness whereas light with opposite handedness is transmitted.^[6] Normally, such coloring mechanism mainly originates from the multilayer structure of helically stacked chitin microfibrils.^[7] Nevertheless, some of these striking color appearances are due to the coupling effects of different photonic components within one hierarchical architecture,^[8–10] showing synergistic combinations of

structure-imposed optical behavior and intrinsic material properties.

Retroreflection is a special type of reflection that differ from diffuse and mirror reflection, which can reflect light along its incident direction over a continuous range of incident angles. A common way to enhance the visibility of photonic structure involves coupling with a layer of transparent retroreflective elements.^[11,12] Upon illumination, light travelling within the retroreflective material reflects light with high efficiency along its incident direction, making the structural color conspicuous and dazzling under dim-light environment.^[13–15] While microlens array (MLA) is another kind of micro-optical system that contains patterned miniaturized lenses with diameters ranging from several micrometers to nearly a millimeter.^[16] Conventional MLAs usually rely on the specific phase accumulation of light along the propagation in isotropic media, with their focusing effects controlled by the shape and curvature of each individual microlens.^[17–19] Polarization-sensitive MLA structures, like those of insect's compound eyes and calcite crystal array in brittlestars,^[20,21] exist ubiquitously in nature. Taking *Chrysina gloriosa* as an example, the chitin fibrils in the carapace are organized into a cholesteric focal conic texture with a cellular polygonal pattern,^[22] acting as MLA to perform polarization-sensitive beam shaping that relies on the intrinsic helical organization.^[23] These polygon cells have concave shapes with a transparent layer of wax-filled outer cuticle.^[24] Light penetrating through the wax layer is anomalously reflected back to

1. Introduction

Structural color is common among living creatures. Interestingly, human eye can only perceive the hue, brightness, and

Dr. G. Chu, Dr. F. Chen, B. Zhao, Dr. X. Zhang, Prof. O. J. Rojas

Department of Bioproducts and Biosystems

School of Chemical Engineering

Aalto University

P.O. Box 16300, Aalto, Espoo FI-00076, Finland

E-mail: chuguang88@gmail.com; orlando.rojas@ubc.ca

Prof. E. Zussman

NanoEngineering Group

Faculty of Mechanical Engineering

Technion – Israel Institute of Technology

Haifa 3200003, Israel

Prof. O. J. Rojas

Departments of Chemical and Biological Engineering, Chemistry

and Wood Science

Bioproducts Institute

The University of British Columbia

2360 East Mall, Vancouver, BC V6T 1Z3, Canada

 The ORCID identification number(s) for the author(s) of this article can be found under <https://doi.org/10.1002/adom.202002258>.

© 2021 The Authors. Advanced Optical Materials published by Wiley-VCH GmbH. This is an open access article under the terms of the Creative Commons Attribution-NonCommercial License, which permits use, distribution and reproduction in any medium, provided the original work is properly cited and is not used for commercial purposes.

DOI: 10.1002/adom.202002258

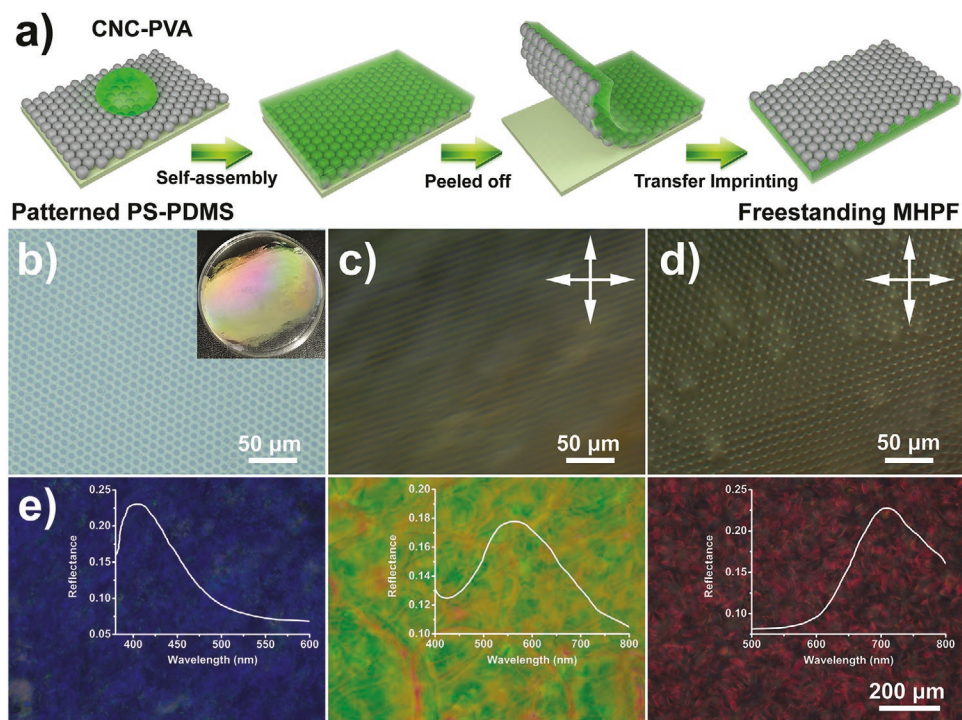


Figure 1. a) Schematic representation of the transfer imprinting method to prepare a micropatterned MHPF. b) Optical image of the prepared micropatterned PS microspheres (10 μm) on a PDMS substrate. Inset is the optical image of the PS–PDMS mold which shows strong interference color upon directional light impinging. c,d) POM images of the drying process of CNC–PVA suspension on the micropatterned PS–PDMS substrate, showing aligned cholesteric fingerprint texture along the PS microsphere array. e) Optical image of MHPF1–3 (PS 10 μm) that focuses on the upper smooth surface, displaying optically tunable cholesteric CNC matrix that varies from blue, green to red. The insets are the corresponding UV–vis spectra, respectively.

the direction from the bottom center of the cells, representing as micrometer-sized retroreflective axicon.^[25] Inspired by the natural example, we therefore hypothesize the possibility of designing an artificial optical device that combines the microscopic retroreflector and MLA element within self-assembled nanoscopic helicoid structure, which can enlarge the scope of integrated photonics with multiple functions.

Being one of the most abundant biopolymers on the biosphere, some cellulosic structures are known for their brilliant iridescence through helicoidally structured cellulose nanomaterials in plants.^[26,27] Cellulose nanocrystals (CNCs) isolated from plant material, for example, through acid hydrolysis, show twisted rod-like morphologies with excellent colloidal stability in aqueous media.^[28–30] Upon evaporation, colloidal CNC particles spontaneously self-assemble into a cholesteric liquid crystal phase above critical concentration and further vitrify into solid film that retain the original helical structure, thereby yielding vivid structural color with tunable photonic band gap.^[31,32] Owing to the nanometer-sized building blocks and robust self-assembly process, cholesteric ordered CNC can serve as versatile platform for material templating,^[33,34] nanoimprinting,^[35–38] matrix scaffolding,^[39–42] and colloid assembly,^[43–46] which can allow the construction of hierarchical photonic structures with precisely controlled light–matter interactions.

Herein we introduce a straightforward approach to fabricate micropatterned photonic films that combines cholesteric self-assembly of CNC and monolayer array of polystyrene (PS) microspheres, presenting as integrated polarization-sensitive

retroreflector and MLA. We use aqueous CNC suspension as the lithography ink that is cast onto a pre-engineered polydimethylsiloxane (PDMS) mold with surface structured PS microspheres. After drying, iridescent cholesteric films are obtained with subtle micropatterned bottom surface replicated from the PS microsphere array. When a beam of light interacts with the micropatterned surface, the embedded PS microspheres act as retroreflective array that enhances the structural color of the cholesteric CNC matrix, displaying varying visibilities, depending on the viewing and illumination angles. On the contrary, when the incident light penetrates through the bottom anisotropic cholesteric CNC layer and impinging onto the upper isotropic PS microspheres, a geometric-induced planoconvex MLA is formed, exhibiting remarkable polarization-sensitive imaging performance. This simple design to produce the multifunctional photonic device, offering a general framework to manipulate the flow of light within hierarchical architecture that may be of interest for both fundamental and applied research.

2. Results and Discussion

In order to prepare the multifunctional hybrid photonic films (MHPFs) containing a bulk cholesteric CNC matrix and monolayer of PS microsphere surface array, we anticipate a simple evaporation-assisted transfer imprinting approach for large-area patterning of monodisperse spherical particles (Figure 1a).

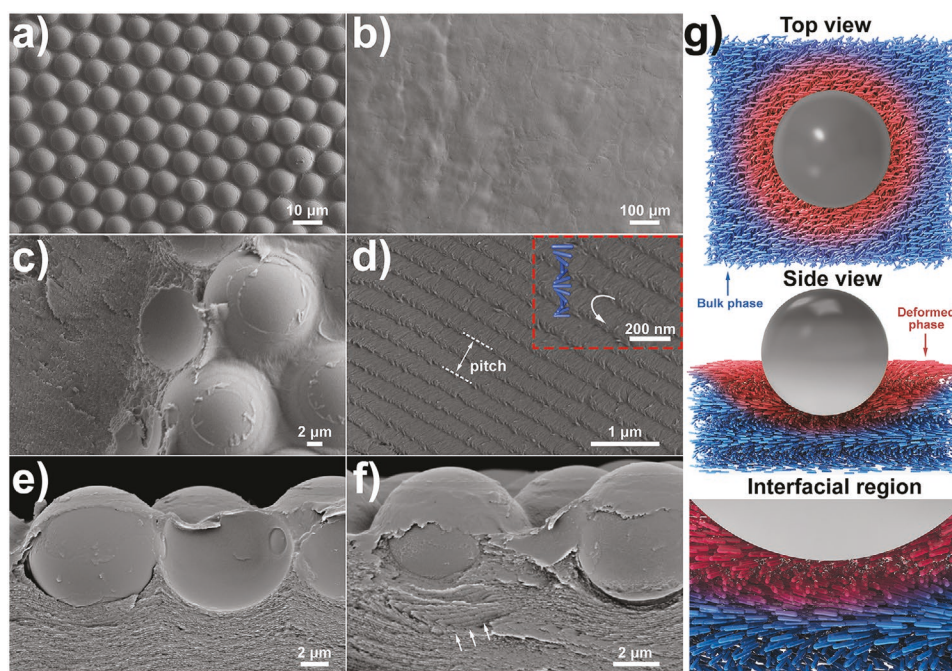


Figure 2. Morphology of an MHPF2 composite produced with PS microspheres (diameter of 10 μm). Top view SEM image of MHPF2 with a) a bottom, micropatterned surface and b) an upper, smooth surface. c) Low magnified SEM image of MHPF2 focusing on the fractured region, showing a smooth inner surface of CNC–PS interface and layered organization of CNC in the bulk phase. d) High-magnification SEM image of the layered structure in the bulk phase. The inset highlights the left-handed twisted assembly of CNC nanoparticles. e, f) Side view of the interface between PS microspheres and the bulk phase, showing distorted layer structures around the microspheres. The arrows in (f) highlight the topological defects near the CNC–PS interface. g) Illustration of the hierarchical structure of MHPF composite showing a cholesteric bulk phase and a volume-induced distortion around a PS microsphere.

In brief, an aqueous CNC suspension (5.0 wt%, zeta potential -48 mV, 15 nm in diameter, and 300–400 nm in length) with varying sonication times (ranging from 2 to 15 min) was mixed with a fixed value of polyvinyl alcohol (PVA, mass ratio 1:1). After stirring at room temperature for 1 h, the resulting mixture was poured on top of a preprepared micropatterned PS–PDMS mold and left to dry under ambient conditions, forming a system that is therein referred to as MHPF1–3 (Table S1, Supporting Information). Closely packed, hexagonal array of PS microspheres was first assembled on PDMS substrate through unidirectional rubbing of a dry particle powder with different sizes (5.0 ± 0.15 , 10.0 ± 0.1 , and 15.1 ± 0.26 μm) between two rubber plates,^[47] exhibiting microscopic single-crystal colloidal monolayer with strong interference-induced structural color (Figure 1b and Figures S1–S3, Supporting Information). Then the PS–PDMS mold was treated with oxygen plasma to partially make the microsphere surface hydrophilic and more suitable for suspension casting. We further tracked the evaporation process of CNC–PVA suspension on the PS–PDMS template through a series of polarized optical microscopy (POM) images (Figure 1c,d and Figure S4, Supporting Information). The obtained results revealed that the cholesteric fingerprint texture was confined and aligned along the convex interface of PS microspheres. After evaporation and peeling off the samples from the template, free-standing MHPFs were obtained with an upper smooth cholesteric surface and a bottom patterned PS microsphere array that was transferred from the PDMS substrate. Contrary to the otherwise hydrophobic PS/PDMS interface, the transfer assembly is formed by the strong interfacial

adhesion achieved between the CNC matrix and the pretreated hydrophilic PS surface.^[14] Normal view of the film's upper surface shows a series of tunable structural colors (blue, green, and red) and varying photonic band gaps (405, 560, and 710 nm), which can be ascribed to the increased helical pitch (Figure 1e and Table S2, Supporting Information). Compared to the neat CNC suspension, the addition of PVA can highly improve the mechanical strength of the final composite films, switching from stiff and brittle to ductile and flexible,^[35] showing great potential as a self-organized adhesive tape for a crack-free particle transfer imprinting process. Furthermore, the organization of PS microspheres array can be readily achieved by modifying the surface adhesion of PDMS substrate, therefore, transferred into the CNC matrix with designed patterning (Figure S5, Supporting Information).

The surface morphology and inherent cholesteric organization were characterized by scanning electron microscopy (SEM). A case study considering MHPF2 with PS diameter of 10 μm featured a micropatterned, long-range hexagonal packing with plano-convex hemispherical morphology at the bottom surface, whereas the upper side of film was particle-free and glossy (Figure 2a,b). Fractures perpendicular to the film surface showed a smooth inner surface at the cavity of the PS microspheres and the lamellar twisted CNC structure in the bulk phase, which implied a planar anchoring of CNC around the PS microsphere (Figure 2c,d and Figure S6, Supporting Information). The CNC director in the bulk matrix rotated in a left-handed direction, consistent with cholesteric organization and was responsible for the selective reflection of light.^[6,31]

Looking at the cross-sections of the film, the layered cholesteric structure was varied along the curved PS interface, confirming the deformed planar anchoring of CNC at the particle interface during evaporation (Figure 2e and Figure S7, Supporting Information).^[48] Meanwhile, the PS microspheres could distort the spatial ordering of liquid crystalline CNC matrix, creating topological defects (e.g., dislocations and disclinations) in the cholesteric matrix close to the particle surface (Figure 2f). Such effects result from the capillary forces that develop between neighboring PS microspheres, given that during the drying process the evaporation rate at the bulk cholesteric phase is faster than that at the CNC–PS interfacial region. The calculated helical pitch near the PS interface was 300 ± 10 nm, smaller than the helical pitch in the bulk region (380 ± 10 nm), which was ascribed to the kinetic arrest of cholesteric organization during the confined drying process.^[49] Varying the size of the PS microspheres embedded into CNC matrix through evaporation-assisted transfer imprinting process, facilitates the display of close-packed particle arrangement that is given by the initial PS–PDMS substrate (Figure S8, Supporting Information). Thus, we conclude that the PS microspheres have dimensions orders of magnitude larger than the CNC nanoparticles and their helical assembly, which enables the cholesteric liquid crystal phase to be retained in the bulk matrix and to be deformed around the PS template.^[50] In addition, the coassembly of PS microsphere into CNC matrix can be manipulated through the time used for plasma treatment, giving rise to a less embedded (contact angle $< 90^\circ$) or a completely embedded (contact angle $> 90^\circ$) PS microsphere array with varying curvatures (Figure S9, Supporting Information), providing a tailor-able platform for the transfer imprinting process.

Based on the above, Figure 2g is sketched to illustrate the hierarchical organization of CNC nanoparticles around PS microspheres in MHPF composite. During the drying process, the volume fraction of CNC particles continuously increases and eventually self-assemble into a cholesteric glassy state.^[51] Owing to the elastic interplay between cholesteric CNC and hydrophilic particle surface, the PS microsphere will deform the liquid crystal interfacial region and generate a nontrivial interfacial curvature with bend-splay orientation distortions around the PS surface.^[46,52] However, in the bulk region which far away from PS microspheres, the CNCs are freely assembled with the bulk helix appear to be oriented normal to the film surface.^[49] As a result, the spatial ordering of cholesteric matrix is distorted around the curved hydrophilic PS surface, with the CNC orientation takes on a planar arrangement to lower the anchoring energy,^[48] leading to long-range periodic assembly in the bulk phase and a deformed helical organization at the CNC–PS interface, with these arrangements further arrested in solid film.

Shining light onto the micropatterned CNC–PS surface produced vivid structural color due to the selective reflection of cholesteric matrix and retroreflection of the incident light along the PS microsphere. **Figure 3a** shows the optical signature of the MHPF sample upon light illumination. The micropatterned surface of MHPF2 composite displayed an opaque white appearance under indirect diffuse illumination, whereas the PS-free area showed vivid greenish structural color that resulted from the helical organization of the CNC matrix. By contrast,

upon directional illumination, the patterned PS area turned into a luminous blue with glittery appearance, revealing the photonic coupling between retroreflection and circularly polarized selective reflection in the micropatterned PS area. Similar optical shifting trends were observed in other samples with different pitch and size of PS microspheres (Figures S10 and S11, Supporting Information). Furthermore, the patterned PS region exhibited vivid structural color with enhanced visibility and conspicuity under left-handed circularly polarized (LCP) illumination, while the same pattern taken under right-handed circularly polarized (RCP) illumination was inconspicuous (Figure 3b), implying selective reflection of circularly polarized light with specific handedness. Apart from polarization, the retroreflection signals depended on the viewing and illumination angles, showing angular-dependent response upon non-coaxial illumination and angular-independent response with coaxial condition (Figure S12, Supporting Information). Owing to the PS microspheres in close proximity to the cholesteric CNC matrix, the obtained photonic coupling (retroreflection and selective reflection) cannot be macroscopically resolved, instead, they merged together to create an additive effect on illumination-induced structural color, which presented distinctive glittery colored appearance.

To investigate how the retroreflection occurs at the microscopic CNC–PS interface, the MHPF composite was further analyzed in reflection mode, with light source directed normal to the film surface. A previous report demonstrates that the ratio of particle size and incident light wavelength (D/λ) has a strong influence on retroreflective light intensity.^[53] Indeed, the retroreflection signal is suppressed when the size of the PS microspheres (D) is smaller than the incident wavelength (λ). By contrast, the retroreflection signal increases when D is between two- and fourfold greater than λ , reaching a maximum intensity when $D \gg \lambda$. Sweeping the focus plane of MHPF3 surface at different depths led to varied reflected signals through the embedded PS microsphere (diameter of 15 μm , Figure 3c and Movie S1, Supporting Information). The micropatterned surface was blurry when we focused on the upper and lower edge of the PS microsphere, characteristic for imaging out-of-focus. The central reflection spot was observed at the depth that focused on the top edge of PS microspheres, whereas a radial peripheral light pattern was formed by focusing the inner part of the PS microspheres, due to the light reflection toward neighboring microspheres.^[54] Therefore, the transparent PS microsphere acted as ball lens retroreflectors on the cholesteric matrix, resulting in illumination-induced glittery colored appearance due to the light reflection from PS–CNC interface, rather than interference from the surface array. MHPF samples with varied helical pitch of CNC matrix and different PS microsphere size presented similar optical signatures (Figures S13 and S14, Supporting Information). As a comparison, Figure 3d shows the optical signatures of micropatterned surface under different polarized illumination states that in focus. In specific, the central reflection spot disappeared under crossed polarized state and the transparent PS layer still remained birefringent, owing to the bottom cholesteric CNC matrix. This phenomenon can be ascribed to the optical extinction of reflected linearly polarized light with a perpendicular polarization direction with respect to the analyzer. By contrast, POM images taken

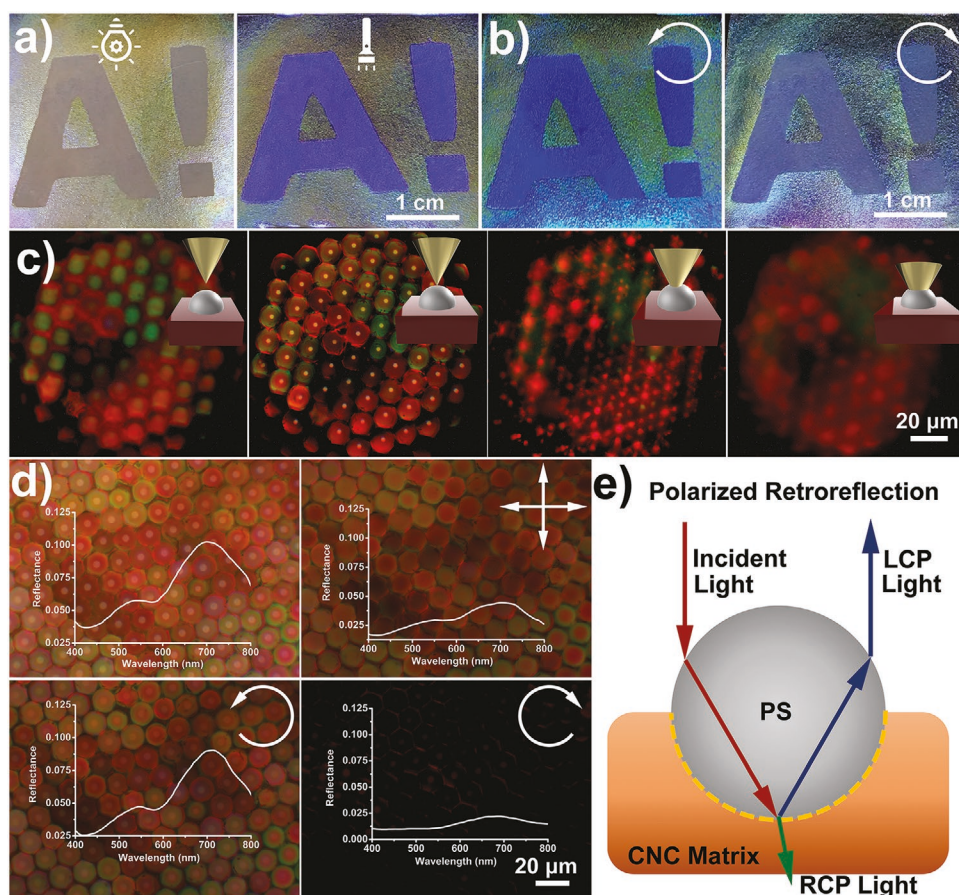


Figure 3. a) Photographs of PS microspheres (15 μm) in MHPF2 under indirect diffuse illumination (left) and directional illumination (right). The PS particles are assembled into an “A!” shape to highlight the micropatterned surface. b) Photographs of MHPF2 under directional LCP (left) and RCP (right) illuminations, respectively, showing the polarization-sensitive retroreflected structural color. c) Optical images of MHPF3 that focus on the micropatterned surface at different focus planes. The insets correspond to the focus planes at the PS–CNC surface. d) Regular optical image and POM images of the MHPF3 micropatterned surface with linear-crossed, LCP and RCP polarizer. Insets are their corresponding UV–vis spectra under different polarization states. e) Schematic description of the polarization-sensitive retroreflection. The incident light splits into LCP and RCP parts at the PS–CNC interface with the LCP light reflecting along its incident direction.

with circular polarizations showed that the CNC–PS retroreflector predominantly reflected LCP light while the RCP counterpart penetrated through the CNC matrix. The polarized UV–vis spectra presented double-peak spectral feature at 540 and 710 nm for unpolarized and LCP states and suppressed under crossed-polarized and RCP states (Figure 3d, inset), revealing polarization-sensitive reflections in micropatterned surfaces. Therefore, we suggested that there occurred a strong light–matter interaction between cholesteric CNC matrix and embedded PS microsphere, namely, the photonic coupling of selective light reflection and retroreflection.

A sketch of the proposed optical mechanism for polarized light retroreflection is shown in Figure 3e. For small incident angles, the retroreflective results are close to those at normal incidence due to the cylindrical symmetry of the PS beads around the optical axis of the incident beam (Figure S15, Supporting Information), whereas symmetry broken occurs for the scattered background light at larger angles.^[55] When the incident light reaches the upper surface of the transparent PS array, it will be first refracted at the air–PS interface, then penetrating to the lower surface of the PS layer and be further

selectively reflected at the CNC–PS interface. This interfacial region acts as a concave spherical mirror with required curvature for retroreflection with specific polarization.^[56] The LCP light that matches the handedness of cholesteric CNC matrix is internally reflected back through the frontal surface of PS microsphere and refracted in a direction parallel to its origin, whereas the RCP portion of the incident light passes through the cholesteric CNC matrix.^[6] As a comparison, the retroreflection signal for a cholesteric-free CNC–PS reference sample is negligible (Figure S16, Supporting Information), which is a consequence of the small difference in refractive index between PS microsphere ($n_{\text{PS}} = 1.59$) and cholesteric-free CNC matrix ($n_{\text{CNC}} = 1.56$). When light propagates from the PS layer into the CNC matrix, the reflectivity (R) of the interfacial region can be expressed by the Fresnel equation^[57] $R\% = [(n_{\text{PS}} - n_{\text{CNC}})/(n_{\text{PS}} + n_{\text{CNC}})]^2 \times 100$ and calculated to be 0.009%, implying that most of incident light is transmitted. Based on this, the cholesteric matrix at the CNC–PS interface appears to play a critical role in retroreflection, namely, the incident light is selectively split into opposite circularly polarized states with enhanced reflectivity (up to 50%), leading to chiral light–matter interactions

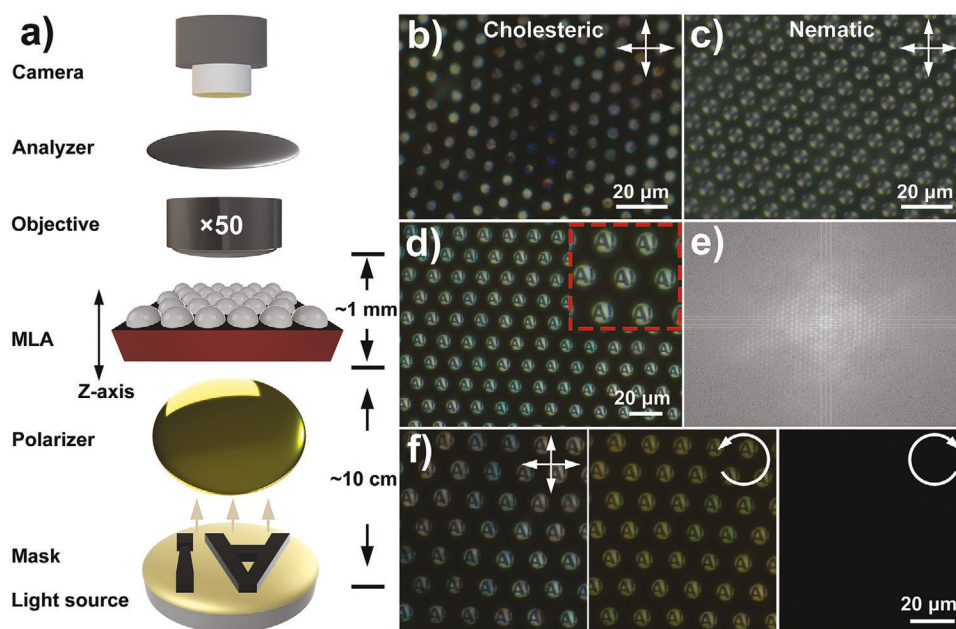


Figure 4. Optical imaging performance of MHPF sample as polarization-sensitive MLAs. a) Schematic setup of the optical system for imaging a centimeter-sized mask of inverted “A!”. POM images of the MLAs composed by b) cholesteric and c) nematic CNC matrix, respectively. The PS microspheres in each MLAs are 15 μm and illuminated without mask. d) Optical image of the “A!” array projected by MHPF3 with PS diameter of 15 μm . Inset is the magnified image array with high projecting quality. e) The Fourier transformed images from (d). f) POM images of the “A!” array projected under linear-crossed, LCP and RCP polarizers (MHPF3 with PS diameter of 15 μm), showing polarization-dependent imaging performance.

at the CNC–PS interface and serving as polarization-sensitive microarray.

Instead of light impinging on the micropatterned PS surface for retroreflection, when collimated light beam is directed on the smooth cholesteric CNC matrix and passed through PS layer, the transmitted light converges into the common image plane of each individual microspheres, thereby resulting in a plano-convex MLA. The focal length f in the MHPF sample is polarization independent and determined by the size of the embedded PS microspheres, $f = n_{\text{CNC}}R/(n_{\text{PS}} - 1)$ where R is the radius of curvature that can be estimated as the radius of PS microsphere.^[6] Thus, the calculated focal length for MHPF samples with varying size of PS microspheres (5, 10, and 15 μm) are 13.2, 26.4, and 39.6 μm , which, in turn, the corresponding MLAs are able to concentrate light and project image at varying image planes. To inspect the optical microlens property of the MHPF sample, a projection experiment was performed with a homemade optical setup that shown in **Figure 4a**. The MHPF sample was placed on the microscope stage with the convex PS surface against the objective and illuminated with white light through a projection mask with ≈ 1.5 cm in size, then scanned along the z -direction of the microscope. The $z = 0$ position was defined as the MLA top surface located at the microscope objective focus and no diffracted image array was observed from the MLA (Figure S17, Supporting Information). Clear projected image array was observed when the focal point of the objective lens was moved to the focal plane of the MLA (positive z position), whereas blurred image array was either underfocused or overfocused (Figure S18, Supporting Information). Figure S19 in the Supporting Information presented the focused light spot image and the corresponding light intensity distribution for

MHPF sample with different sizes of PS microspheres. The light spots in an orderly fashion had the same peak intensity, which implied the uniformity of the MLA.

To evaluate polarization imaging property, we compared the MHPF sample (cholesteric CNC matrix with PS microsphere array) with cholesteric-free reference sample (nematic CNC matrix with PS microsphere array) under crossed polarizers and without mask illumination. Owing to the structural differences in the CNC matrix, the POM image of the MHPF-derived MLA showed birefringence in each microlens, whereas the cholesteric-free reference MLA presented an array of Maltese cross-like pattern (Figure 4b,c and Figure S20, Supporting Information). When the linearly polarized light was directed on the MHPF sample, the incident light passed through the cholesteric matrix and turned into RCP state that could further propagate through the analyzer. Whereas the crosspattern could be ascribed to the nematic ordered CNC–PS microlens that modulated by both linearly polarized incident light and orthometric analyzer.^[58] Furthermore, a hexagonal array of inverted virtual images “A!” was clearly captured upon masked illumination, which was due to the convex structure of the MHPF surface, capable of focusing light (Figure 4d). The projected images were 5.5 μm in size and uniform in shape, which was 2700 times smaller than the projected object, implying the uniformity and accurate surface topography of the MLA system. This could also be confirmed by a Fourier transformation analysis of the image, which showed discrete dot patterns due to the uniform and well-ordered repeating units (Figure 4e). Tuning the size of PS microsphere in MLA and object distance in projecting system would effectively manipulate the size of image array

and ensure high-resolution imaging capability (Figure S21 and Movie S2, Supporting Information). In addition, on account of the birefringent characteristic of cholesteric CNC matrix, the obtained MLAs demonstrated pronounced polarization-sensitive imaging. The projected image array was clearly visible under crossed-polarized and LCP illumination but fully extinguished under RCP illumination (Figure 4f), revealing that the interior CNC cholesteric structure endowed chiral modulation to the transmitted light and exhibited polarization-sensitive focus plane. On the contrary, the reference cholesteric-free MLA displayed a polarization-independent imaging performance under LCP and RCP illumination and deformed image array under crossed polarizers (Figure S22, Supporting Information). Therefore, these unique MLAs made of anisotropic CNC matrix and micropatterned isotropic PS microspheres offered a general platform for the developing of polarization-dependent micro- and nano-optics.

3. Conclusion

To conclude, we have developed a new kind of photonic structure composed of optically tunable cholesteric CNC matrix and micropatterned PS microsphere surface array. In the present work, both bottom-up and top-down approaches were combined in the transfer imprinting process. This includes CNC self-assembled into a helical organization and an adhering monolayer of PS microspheres from the pre-engineered PDMS mold. The system departs from any previous constructs given the integration of retroreflector and MLA into a single photonic structure, allowing a better understanding of the chiral light-matter interactions in MHPF, e.g., arising from a hierarchically organized CNC-PS binary structure. The latter acts as a photonic retroreflector platform that results in vivid structural color with enhanced visibility while incorporating the MLA functionality for light focusing and to project miniaturized image arrays. The ease of fabrication, scalability of the micro-nano transfer imprinting method, together with custom-tailored photonic structure, will make the micropatterned MHPF concept particularly attractive for multifunctional optical devices, bearing great potential for metamaterial design and fabrication.

4. Experimental Section

Preparation of PDMS Substrate: The PDMS support used for rubbing was prepared with conventional prepolymer and curing agent (a weight ratio of 10:1 was used to increase friction with the PS microparticles). For the PDMS substrate used for particle coating, a weight ratio of 2:1 was used, which reduced the particle-substrate adhesion energy and facilitated contact between PS microparticles and the PDMS substrate.^[59] In brief, 5.0 g of the mixture was poured onto a Petri dish (60 mm diameter) with a PDMS layer of 2 mm thickness. Afterward, the mixture was degassed in a vacuum oven at room temperature for 20 min and crosslinked in an oven at 70 °C for 3 h.

Preparation of Single Crystal Monolayer of PS Microsphere on PDMS Substrate: Typically, a freshly prepared PDMS substrate (weight ratio of 2:1) was fixed on the stage. After placing a small amount of PS powder (0.01 g), the bottom support was covered with an PDMS-coated (weight ratio of 10:1) glass and rubbed back and forth (30 times) in the in-plane direction under a loading pressure and moving speed of 10^5 Pa and

5 mm s^{-1} . Then, the residual particles were blown off by compressed air flow, resulting in a monolayer array of PS microparticles.^[47] In order to hydrophilize the topmost section of the PS microparticle layer and PS-free PDMS substrate, the prepared micropatterned PS-PDMS substrate was placed in a plasma vacuum chamber (Diener Surface Plasma Cleaner, Pico) for oxygen plasma treatment at 250 mTorr for a given time (10 s, 2 min, and 5 min, respectively). Following this procedure, a partially hydrophilic monolayer of PS microspheres was obtained on the surface of the PDMS substrate (with the bottom section comprising the hydrophobic side of the PS array). This system was then used as template for the transfer-imprinting process.

Preparation of Patterned PS Microspheres on PDMS Substrate: The patterned PS-PDMS support was prepared by a selective ultraviolet oxidation treatment, as reported by Park et al.^[60] Briefly, the cured PDMS substrate (2:1) was covered with a homemade mask (letter "A!") and exposed to ultraviolet-ozone for 60 min to decrease the adhesion energy of the uncovered PDMS surface. Following, the mask was removed and the PS microspheres were assembled on the PDMS support by using the same procedure as that used for directional rubbing. Then, the excess amount of PS microspheres was blown off by compressed air flow. Due to the differences in the adhesion energy between masked and unmasked PDMS supports, the PS microspheres presented stronger interactions with the masked PDMS support and resulted in the formation of the mask pattern upon flowing compressed air. Finally, the prepared patterned PS-PDMS substrate was placed in a plasma vacuum chamber (Diener Surface Plasma Cleaner, Pico) for an oxygen plasma treatment (2 min) to make the uppermost layer hydrophilic, to facilitate the transfer-imprinting process.

Preparation of CNC Suspension: In a typical experiment, 50 g of bleached soft wood pulp was milled using a commercial pulper containing 1000 mL of deionized water, followed by oven-drying. Next, 20 g of milled pulp was hydrolyzed in 200 mL of H_2SO_4 (1g pulp/10 mL H_2SO_4) aqueous solution (64 wt%) under vigorous stirring at 45 °C for 60 min. The pulp slurry was diluted with cold deionized water (about ten times the volume of the acid solution used) to stop the hydrolysis and allowed to subside overnight. The clear top layer was decanted and the remaining cloudy layer was centrifuged. The supernatant was decanted and the resulting thick white slurry was washed three times with deionized water. Finally, the white thick suspension was placed into a Millipore ultrafiltration cell (model 8400) to wash the cellulose nanocrystals with deionized water until the pH of solution was stable at 3 (usually take 4–5 d). The thick pulp slurry from the Millipore cell was diluted to 5 wt% and sonicated for 2, 5, and 10 min, for further usage.^[40]

Preparation of MHPF Composites: Typically, an aqueous CNC suspension (5 g, 5.0 wt%) was mixed with 0.25 g PVA powder (CNC:PVA weight ratio of 1:1) and stirred at room temperature for 3 h to allow for the formation of a homogeneous mixture, which was used as CNC-PVA ink for transfer-imprinting. Then, the ink was transferred onto the surface of the preprepared micropatterned PS-PDMS substrate (PS diameter of 5.0 ± 0.15 , 10.0 ± 0.1 , $15.1 \pm 0.26 \mu\text{m}$) and allowed to evaporate under ambient conditions to form solid films on the surface of PDMS (typically after ≈ 2 d), generating CNC-PVA composite with cholesteric ordering. Finally, the CNC-PVA films was carefully peeled off from the PS-PDMS substrate with the micropatterned PS microspheres imprinted onto the bottom surface of the film, giving rise to free-standing micropatterned CNC-PS films. Depending on the sonication time of the initial CNC suspension (2, 5, 10 min), the resulting composites are herein referred to as MHPF1, MHPF2, and MHPF3 with the respective structural color being blue, green, or red. The corresponding PS-free composites were used as reference samples (referred to as REF1, REF2, and REF3) and prepared following the same conditions, casting the CNC-PVA ink onto plasma treated PDMS sheet with a smooth surface, in the absence of PS microspheres.

As a comparison, a micropatterned CNC-PS composite film without cholesteric ordering was prepared by casting an ink consisting of CNC-PVA and NaCl onto a wrinkled PDMS mold, following a similar process as that described above. Typically, the ink was prepared by mixing PVA (0.25 g) with an aqueous CNC suspension (5 g, 5.0 wt%) through vigorous stirring for 1 h

and then NaCl was added into the mixture for a final concentration of 5×10^{-3} M. Afterward, this CNC–PVA–NaCl ink was casted onto micropatterned PS–PDMS substrate for 2 d to generate a CNC–PS composite film with nematic ordering (cholesteric-free) on the micropatterned surface.

The preparation process used to engineer patterned MHPF followed that of the regular MHPF sample. Typically, the CNC–PVA ink (CNC 5 g, 5.0 wt%; PVA 0.25 g) was casted onto the micropatterned PS–PDMS substrate with engineered surface pattern (letter “A!”). After the CNC–PVA composites were dried, peeling off the film imprinted the PS microsphere array into the cholesteric CNC–PVA film, leading to a free-standing engineered MHPF.

Supporting Information

Supporting Information is available from the Wiley Online Library or from the author.

Acknowledgements

This work was a part of the Academy of Finland's Flagship Programme under Projects Nos. 318890 and 318891 (Competence Center for Materials Bioeconomy, FinnCERES). G.C. acknowledges the financial support from the Novo Nordisk Foundation (Grant No.: NNF200C0064350). O.J.R. acknowledges support by the Canada Excellence Research Chair initiative, the Canada Foundation for Innovation (CFI), and the European Research Council (ERC) under the European Union's Horizon 2020 research and innovation program (ERC Advanced Grant Agreement No. 788489, “BioElCell”). Sincere gratitude goes to Prof. Silvia Vignolini and Thomas Parton for valuable discussion.

Conflict of Interest

The authors declare no conflict of interest.

Data Availability Statement

The data that supports the findings of this study are available in the supplementary material of this article.

Keywords

cellulose nanocrystals, microlens arrays, patterned materials, photonic crystals, retroreflection

Received: December 29, 2020

Revised: January 23, 2021

Published online: February 22, 2021

- [1] G. Horváth, D. Varju, *Polarized Light in Animal Vision: Polarization Patterns in Nature*, Springer Science and Business Media, Berlin, Germany **2004**.
- [2] A. D. Briscoe, L. Chittka, *Annu. Rev. Entomol.* **2001**, *46*, 471.
- [3] I. M. Daly, M. J. How, J. C. Partridge, S. E. Temple, N. J. Marshall, T. W. Cronin, N. W. Roberts, *Nat. Commun.* **2016**, *7*, 12140.
- [4] K. Cheng, *Arthropod Navigation: Ants, Bees, Crabs, Spiders Finding Their Way*, Oxford University Press, Oxford **2012**.
- [5] T. W. Cronin, N. Shashar, R. L. Caldwell, J. Marshall, A. G. Cheroske, T. H. Chiou, *Integr. Comp. Biol.* **2003**, *43*, 549.

- [6] H. De Vries, *Acta Crystallogr.* **1951**, *4*, 219.
- [7] Y. Bouligand, *Tissue Cell* **1972**, *4*, 189.
- [8] L. T. McDonald, E. D. Finlayson, B. D. Wilts, P. Vukusic, *Interface Focus* **2017**, *7*, 20160129.
- [9] S. Caveney, *Proc. R. Soc. London, Ser. B* **1971**, *178*, 205.
- [10] S. A. Jewell, P. Vukusic, N. Roberts, *New J. Phys.* **2007**, *9*, 99.
- [11] T. Groszges, *Opt. Mater.* **2008**, *30*, 1549.
- [12] H. Kim, B. Lee, *Opt. Eng.* **2007**, *46*, 094002.
- [13] K. Y. Tsao, H. P. Tsai, K. Y. A. Lin, Y. X. He, H. Yang, *Langmuir* **2016**, *32*, 12869.
- [14] W. Fan, J. Zeng, Q. Gan, D. Ji, H. Song, W. Liu, L. Shi, L. Wu, *Sci. Adv.* **2019**, *5*, eaaw8755.
- [15] Y. Qi, C. Zhou, W. Niu, S. Zhang, S. Wu, W. Ma, B. Tang, *Adv. Opt. Mater.* **2020**, *8*, 2001367.
- [16] P. Nussbaum, R. Voelkel, H. P. Herzig, M. Eisner, S. Haselbeck, *Pure Appl. Opt.* **1997**, *6*, 617.
- [17] J. J. Kim, H. Liu, A. O. Ashtiani, H. Jiang, *Rep. Prog. Phys.* **2020**, *83*, 047101.
- [18] W. K. Kuo, S. Y. Lin, S. W. Hsu, H. H. Yu, *Opt. Mater.* **2017**, *66*, 630.
- [19] W. K. Kuo, G. F. Kuo, S. Y. Lin, H. H. Yu, *Bioinspiration Biomimetics* **2015**, *10*, 056010.
- [20] K. H. Jeong, J. Kim, L. P. Lee, *Science* **2006**, *312*, 557.
- [21] J. Aizenberg, A. Tkachenko, S. Weiner, L. Addadi, G. Hendler, *Nature* **2001**, *412*, 819.
- [22] V. Sharma, M. Crne, J. O. Park, M. Srinivasarao, *Science* **2009**, *325*, 449.
- [23] C. Bayon, G. Agez, M. Mitov, *Lab Chip* **2014**, *14*, 2063.
- [24] G. Agez, C. Bayon, M. Mitov, *Acta Biomater.* **2017**, *48*, 357.
- [25] P. Bouchal, J. Kapitán, M. Konečný, M. Zbončák, Z. Bouchal, *APL Photonics* **2019**, *4*, 126102.
- [26] C. Hébant, D. W. Lee, *Am. J. Bot.* **1984**, *71*, 216.
- [27] S. Vignolini, P. J. Rudall, A. V. Rowland, A. Reed, E. Moyroud, R. B. Faden, J. J. Baumberg, B. J. Glover, U. Steiner, *Science* **2012**, *109*, 15712.
- [28] Y. Habibi, L. A. Lucia, O. J. Rojas, *Chem. Rev.* **2010**, *110*, 3479.
- [29] Y. Ogawa, *Nanoscale* **2019**, *11*, 21767.
- [30] I. Usov, G. Nyström, J. Adamcik, S. Handschin, C. Schütz, A. Fall, L. Bergström, R. Mezzenga, *Nat. Commun.* **2015**, *6*, 7564.
- [31] J. F. Revol, H. Bradford, J. Giasson, R. Marchessault, D. Gray, *Int. J. Biol. Macromol.* **1992**, *14*, 170.
- [32] G. Chu, X. Wang, H. Yin, Y. Shi, H. Jiang, T. Chen, J. Gao, D. Qu, Y. Xu, D. Ding, *ACS Appl. Mater. Interfaces* **2015**, *7*, 21797.
- [33] K. E. Shopowitz, H. Qi, W. Y. Hamad, M. J. MacLachlan, *Nature* **2010**, *468*, 422.
- [34] G. Chu, J. Feng, Y. Wang, X. Zhang, Y. Xu, H. Zhang, *Dalton Trans.* **2014**, *43*, 15321.
- [35] G. Chu, A. Camposeo, R. Vilensky, G. Vasilyev, P. Martin, D. Pisignano, E. Zussman, *Matter* **2019**, *1*, 988.
- [36] G. Chu, D. Qu, A. Camposeo, D. Pisignano, E. Zussman, *Mater. Horiz.* **2020**, *7*, 511.
- [37] A. Espinha, C. Dore, C. Matricardi, M. I. Alonso, A. R. Goñi, A. Mihi, *Nat. Photonics* **2018**, *12*, 343.
- [38] R. Xiong, S. Yu, S. Kang, K. M. Adstedt, D. Nepal, T. J. Bunning, V. V. Tsukruk, *Adv. Mater.* **2020**, *32*, 1905600.
- [39] A. Querejeta-Fernández, G. Chauve, M. Methot, J. Bouchard, E. Kumacheva, *J. Am. Chem. Soc.* **2014**, *136*, 4788.
- [40] G. Chu, X. Wang, T. Chen, J. Gao, F. Gai, Y. Wang, Y. Xu, *ACS Appl. Mater. Interfaces* **2015**, *7*, 11863.
- [41] J. Majoinen, J. Hassinen, J. S. Haataja, H. T. Rekola, E. Kontturi, M. A. Kostianen, R. H. Ras, P. Törmä, O. Ikkala, *Adv. Mater.* **2016**, *28*, 5262.
- [42] G. Chu, X. Wang, T. Chen, W. Xu, Y. Wang, H. Song, Y. Xu, *J. Mater. Chem. C* **2015**, *3*, 3384.
- [43] L. Bai, S. Huan, B. Zhao, Y. Zhu, J. Esquena, F. Chen, G. Gao, E. Zussman, G. Chu, O. J. Rojas, *ACS Nano* **2020**, *14*, 13380.

- [44] B. Frka-Petecic, H. Radavidson, B. Jean, L. Heux, *Adv. Mater.* **2017**, 29, 1606208.
- [45] G. Chu, R. Vilensky, G. Vasilyev, P. Martin, R. Zhang, E. Zussman, *J. Phys. Chem. Lett.* **2018**, 9, 1845.
- [46] G. Chu, R. Vilensky, G. Vasilyev, S. Deng, D. Qu, Y. Xu, E. Zussman, *Angew. Chem.* **2017**, 129, 8877.
- [47] C. Park, T. Lee, Y. Xia, T. J. Shin, J. Myoung, U. Jeong, *Adv. Mater.* **2014**, 26, 4633.
- [48] P. Saha, V. A. Davis, *ACS Appl. Nano Mater.* **2018**, 1, 2175.
- [49] J. H. Park, J. Noh, C. Schütz, G. Salazar-Alvarez, G. Scalia, L. Bergström, J. Lagerwall, *ChemPhysChem* **2014**, 15, 1477.
- [50] C. Blanc, D. Coursault, E. Lacaze, *Liq. Cryst. Rev.* **2013**, 1, 83.
- [51] G. Chu, G. Vasilyev, D. Qu, S. Deng, L. Bai, O. J. Rojas, E. Zussman, *Langmuir* **2020**, 36, 979.
- [52] G. Chu, G. Vasilyev, R. Vilensky, M. Boaz, R. Zhang, P. Martin, N. Dahan, S. Deng, E. Zussman, *Langmuir* **2018**, 34, 13263.
- [53] Y. Kuga, A. Ishimaru, *J. Opt. Soc. Am. A* **1984**, 1, 831.
- [54] J. Fan, Y. Li, H. K. Bisoyi, R. S. Zola, D. K. Yang, T. J. Bunning, D. A. Weitz, Q. Li, *Angew. Chem.* **2015**, 127, 2188.
- [55] D. Héricz, T. Sarkadi, G. Erdei, T. Lazuech, S. Lenk, P. Koppa, *Appl. Opt.* **2017**, 56, 3969.
- [56] Y. D. Han, H. S. Kim, Y. M. Park, H. J. Chun, J. H. Kim, H. C. Yoon, *ACS Appl. Mater. Interfaces* **2016**, 8, 10767.
- [57] T. Takatsuji, M. Goto, S. Osawa, R. Yin, T. Kurosawa, *Meas. Sci. Technol.* **1999**, 10, N87.
- [58] X. Ye, F. Zhang, Y. Ma, L. Qi, *Small* **2015**, 11, 1677.
- [59] Y. Wu, J. Zeng, Y. Si, M. Chen, L. Wu, *ACS Nano* **2018**, 12, 10338.
- [60] C. Park, K. Koh, U. Jeong, *Sci. Rep.* **2015**, 5, 8340.